Anionic amino acids support hydrolysis of poly-β-(1,6)-*N*-acetylglucosamine exopolysaccharides by the biofilm dispersing glycosidase Dispersin B

Received for publication, August 5, 2020, and in revised form, December 14, 2020 Published, Papers in Press, December 17, 2020,
https://doi.org/10.1074/jbc.RA120.015524

Alexandra P. Breslawec, Shaochi Wang, Crystal Li, and Myles B. Poulin*

From the Department of Chemistry and Biochemistry, University of Maryland, College Park, Maryland, USA

Edited by Chris Whitfield

The exopolysaccharide poly-β-(1→6)-*N*-acetylglucosamine (PNAG) is a major structural determinant of bacterial biofilms responsible for persistent and nosocomial infections. The enzymatic dispersal of biofilms by PNAG-hydrolyzing glycosidase enzymes, such as Dispersin B (DspB), is a possible approach to treat biofilm-dependent bacterial infections. The cationic charge resulting from partial de-*N*-acetylation of native PNAG is critical for PNAG-dependent biofilm formation. We recently demonstrated that DspB has increased catalytic activity on de-*N*-acetylated PNAG oligosaccharides, but the molecular basis for this increased activity is not known. Here, we analyze the role of anionic amino acids surrounding the catalytic pocket of DspB in PNAG substrate recognition and hydrolysis using a combination of site-directed mutagenesis, activity measurements using synthetic PNAG oligosaccharide analogs, and *in vitro* biofilm dispersal assays. The results of these studies support a model in which bound PNAG is weakly associated with a shallow anionic groove on the DspB protein surface with recognition driven by interactions with the −1 GlcNAc residue in the catalytic pocket. An increased rate of hydrolysis for cationic PNAG was driven, in part, by interaction with D147 on the anionic surface. Moreover, we identified that a DspB mutant with improved hydrolysis of fully acetylated PNAG oligosaccharides correlates with improved *in vitro* dispersal of PNAG-dependent *Staphylococcus epidermidis* biofilms. These results provide insight into the mechanism of substrate recognition by DspB and suggest a method to improve DspB biofilm dispersal activity by mutation of the amino acids within the anionic binding surface.

In nature, bacteria frequently adopt a sessile life cycle in response to environmental cues that promote the formation of surface-attached biofilms (1). Biofilms consist of bacterial cells embedded in a self-assembled matrix composed of lipids, exported protein, extracellular DNA, and exopolysaccharides that are known collectively as the extracellular polymeric substance (EPS) (2). The exact composition of the EPS varies depending on the bacterial species and on environmental factors, but it serves the same function in all contexts: facilitating cell–cell adhesion and acting as a protective barrier (3–6). Bacterial cells within the biofilm are shielded from the host immune response, decontamination, and are often resistant to common antibiotic treatments (5, 7–9). As a result, biofilms are particularly problematic in hospital settings where biofilm formation contributes to more than half of nosocomial infections (10). Thus, approaches to either prevent biofilm formation or disrupt existing biofilms are being actively pursued to complement traditional antibiotic treatments (11–14).

Exopolysaccharides composed of poly-β-(1→6)-*N*-acetylglucosamine (PNAG) are a major structural constituent of biofilm EPS produced by both Gram-positive and Gram-negative human pathogens including *Staphylococcus epidermidis* (15, 16), *Staphylococcus aureus* (17) *Escherichia coli* (18), *Klebsiella pneumoniae* (19) and *Acinetobacter baumannii* (20, 21). PNAG was first identified in clinical isolates of *S. epidermidis* where it is commonly referred to as polysaccharide intercellular adhesin (PIA) due to its role as a primary biofilm adhesin (15). Two major forms of PNAG have been isolated from *S. epidermidis*. The first is a cationic polysaccharide with approximately 15% of the *N*-acetylglucosamine (GlcNAc) de-*N*-acetylated, and the second is zwitterionic as a result of both partial de-*N*-acetylation and periodic *O*-succinylation of the GlcNAc residues (16, 22). Chemical and enzymatic degradation of PNAG and genetic knockouts of key PNAG biosynthetic genes both result in disruption of biofilms and reduced virulence in animal infection models, highlighting the importance of this polysaccharide for biofilm integrity (8, 16, 18, 19, 23–25). Glycosidase enzymes that specifically hydrolyze PNAG have the potential to be developed as antibiofilm therapeutics as a result of their ability to disperse biofilms (11, 12, 25–27).

There have been two PNAG-specific glycosidase enzymes identified to date: Dispersin B (DspB) (28) and the glycosyl hydrolase (GH) domain of the bifunctional enzyme PgaB (29). DspB is a native β-hexosaminidase enzyme of *Aggregatibacter actinomycetemcomitans* that has been shown to cleave PNAG using both endo- and exoglycosidic cleavage mechanisms depending on the nature of the substrate (28, 30–33). PgaB is the bifunctional carbohydrate esterase/glycosyl hydrolase enzyme required for PNAG biosynthesis in Gram-negative bacteria (24, 34). The PgaB GH domain catalyzes endoglycosidic cleavage of partially de-*N*-acetylated PNAG substrates

* For correspondence: Myles B. Poulin, mpoulin@umd.edu.

containing a glucosamine (GlcN) in the −3 binding site (29, 35). Despite interest in these enzymes as biofilm dispersal agents and as treatments for biofilm-dependent infections, there is still relatively little known about the specific binding interactions required for recognition of their respective PNAG substrates. This is particularly true for DspB. Efforts to engineer more catalytically active variants of DspB as antibiofilm therapeutics would benefit from detailed information about the specific interactions that contribute to substrate recognition and turnover.

In a recent study, we showed that de-*N*-acetylation of PNAG oligosaccharide analogs influences both the mechanism and rate of hydrolysis of DspB for synthetic substate analogs (*i.e.*, **1** and **2**) (33). Specifically, we found that trisaccharide **2** containing GlcN at the +2 binding site showed a nearly threefold faster rate of exoglycosidic cleavage when compared with fully acetylated trisaccharide analog **1**. These results indicate that the substrate cationic charge may contribute to substrate recognition by DspB through interactions with anionic amino acids. Here we use a combination of site-directed mutagenesis, enzyme activity assays with synthetic PNAG substrate analogs, and *in vitro* biofilm dispersal measurements to test this hypothesis and identify amino acids involved in PNAG substrate recognition. These results suggest that mutations outside the DspB catalytic pocket influence PNAG hydrolysis activity and can be used to improve the dispersal of PNAG dependent *S. epidermidis* biofilms by DspB.

Results

Cationic charge increases the rate of substrate cleavage by DspB

Our recent studies of DspB activity using synthetic PNAG trisaccharide analogs with defined acetylation patterns (**1**–**3**) revealed that specific de-*N*-acetylation patterns influence the rate of substrate hydrolysis by DspB (33). Specifically, hydrolysis of the cationic substrate **2** was nearly threefold faster than for either fully acetylated substrate **1** or cationic substrate **3** containing GlcN as the central residue. These results suggest a hypothesis that the increased hydrolysis of **2** may result from specific charge–charge interaction with the cationic GlcN in the +2 binding site (Fig. 1*A*). To test this further, a substrate analog **4** containing glucose (Glc) at the +2 site was synthesized. The acetylation pattern of **4** is the same as that of analog **2** but lacks the cationic charge at the +2 binding site. Analog **4** was synthesized using a one-pot sequential glycosylation approach developed for the synthesis of **1** to **3** (33), as described in detail in the supporting information.

Reaction progress curves for the hydrolysis of **4** by DspB were determined by analyzing the reducing-end product distribution by HPLC (33). This assay allows for quantification of the remaining substrate and reducing-end products resulting from hydrolysis of **4** based on relative HPLC peak areas using the absorbance of the *S*-tolyl aglycone at 254 nm (Fig. 1*B*). The reaction progress curves for hydrolysis of **4** are consistent with sequential exoglycosidic cleavage of the trisaccharide and are consistent with the mechanism observed previously for hydrolysis of **1** to **3** (33). The observed rate of hydrolysis (k_{obs}) was determined by fitting the curve for disappearance of the trisaccharide substrate as a function of time to a single exponential using Equation 1 where $[E_o]$ is the initial enzyme concentration, $[S_o]$ is the initial trisaccharide concentration, and [S] is the trisaccharide concentration remaining at time *t*.

$$[S] = [S_o] \times e^{(-k_{obs}[E_o]t)} \quad (1)$$

The rate of hydrolysis of **4** was nearly identical to that of **1** and **3** and threefold lower than the rate of hydrolysis of

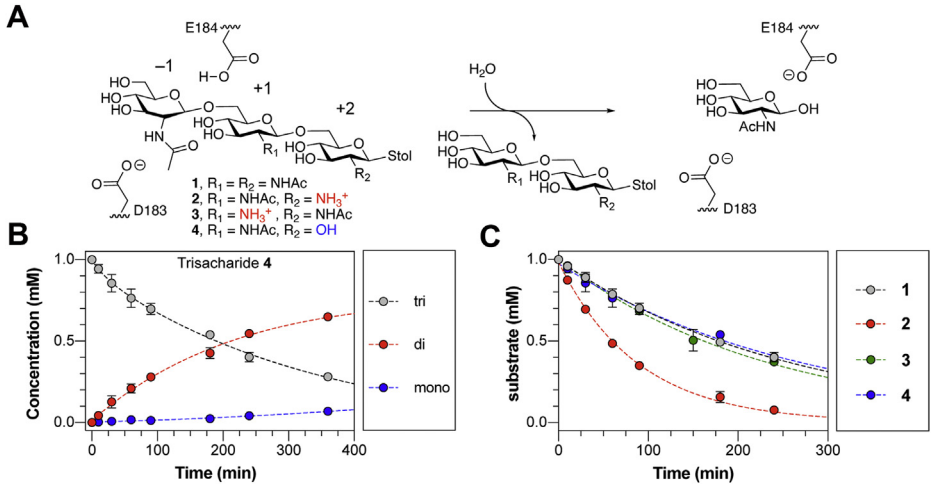

Figure 1. Hydrolysis of PNAG analogs by DspB. *A*, reaction catalyzed by DspB showing the major exoglycosidic cleavage activity for trisaccharide analogs **1** to **4** used in this study. The monosaccharide residues are numbered relative to the site of glycosidic bond cleavage. The position of E184, which serves as a general acid to protonate the leaving group oxygen, and D183, which acts as a base to stabilize the oxazolinium ion intermediate, are shown. *B*, reaction progress curve for the hydrolysis of trisaccharide **3** by DspB. Lines were added to aid identification of the disappearance of the trisaccharide (*gray*) and appearance of reducing-end disaccharide (*red*) and reducing-end monosaccharide (*blue*) products from sequential exoglycosidic cleavage of **4**. Error bars represent the standard deviation from at least two replicate experiments. *C*, relative rates of trisaccharide disappearance for hydrolysis of analogs **1** to **3** by DspB. The rate of trisaccharide disappearance was fit to a single exponential using Equation 1. Error bars represent the standard deviation from two replicate experiments.

cationic analog **2** (Fig. 1*C*). This supports the hypothesis that the increased hydrolysis rate observed with **2** results from recognition of the cationic charge of the substrate and not simply as a result of deacetylation. To further test this hypothesis and determine the specific interactions responsible for recognition of the cationic PNAG analogs, we analyzed the structure of DspB in greater detail.

Negatively charged groove of DspB predicted to bind PNAG

A crystal structure for the DspB apoprotein was reported in 2005 (36), but structural information regarding substrate binding is lacking. DspB is classified as a Family 20 glycosyl hydrolase according to the Carbohydrate Active enZYmes (CAZy) database (37) and adopts a $(\beta/\alpha)_8$ TIM barrel fold, where the predicted catalytic site is found within a pocket ~13 Å deep in the center of the *β*-barrel (Fig. 2*A*) (30, 36). Previous GH20 enzymes have been shown to use a substrate-assisted cleavage mechanism in which the oxygen of the substrate *N*-acetamido group acts as the nucleophile resulting in the formation of an oxazolinium ion intermediate (38). The GlcNAc residue at the site of bond cleavage, the −1 site, adopts an ^{4}E conformation and is contained in a "cage" of conserved aromatic amino acids that serves to orient the *N*-acetamido oxygen for nucleophilic attack (38, 39). Two acidic amino acids flank the glycosidic bond, serving as a general acid protonating the leaving group oxygen (E184 in DspB) and as a "base" to stabilize the oxazolinium ion intermediate (D183 in DspB) (30, 40). The amino acids in the catalytic site are highly conserved among GH20 orthologs, but DspB shares little sequence conservation in the shallow binding surface surrounding the catalytic pocket (Fig. 2*B*) (41). This is not surprising, as the GH20 family contains *β*-hexosaminidase enzymes that have activity on a range of substrates, from chito-oligosaccharides (39) to gangliosides (42) and mammalian *N*-glycan (43, 44). The only GH20 enzymes with confirmed specificity for the *β*-(1→6)-linked GlcNAc of PNAG are the DspB proteins from *A. actinomycetemcomitans* and *Actinobacillus pleuropneumoniae* (28, 45).

Analyzing the electrostatic surface charge of DspB identifies a number of negatively charged amino acids contributing to a shallow anionic groove adjacent to the catalytic pocket (Fig. 2*C*). Three residues in particular, D147, D245, and E248, are located along this anionic groove and are within ~15 Å of the catalytic site, suggesting a possible role in the recognition of cationic PNAG analogs. D147 is located in the loop connecting the β3-sheet and α3-helix and is conserved as an anionic amino acid (Asp or Glu) in the GH20 orthologues that are most similar in sequence to DspB. The remaining two residues, D245 and E248, are located within an extension of the α6-helix that is unique to DspB structure and absent in all other GH20 enzymes crystallized to date (Fig. S1).

In silico *docking simulations support electrostatic protein–substrate interactions*

Further support for the predicted anionic substrate binding surface was obtained from rigid body docking simulations of

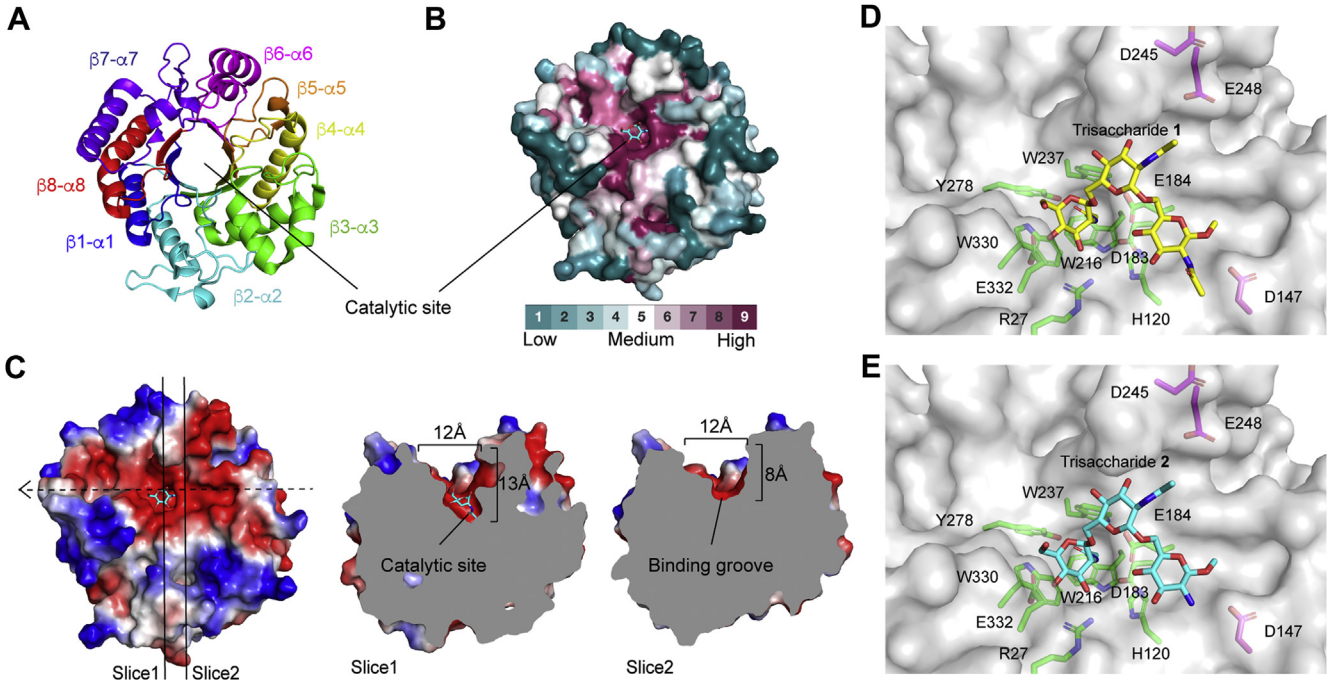

Figure 2. Analysis of the DspB substrate binding surface. *A*, structure of DspB (1HYT) showing the $(\beta/\alpha)_8$ TIM barrel fold with each β-sheet and α-helix pair highlighted. The position of the putative catalytic site is indicated. *B*, surface representation of DspB structure where the residues are colored based on sequence conservation among GH20 orthologs as calculated by Consurf (41). Cyan, white, and fuchsia indicate regions of low, medium, and high sequence conservation, respectively. The position of GlcNAc in the −1 site is shown in cyan sticks. *C*, electrostatic surface map of DspB highlighting a shallow 12 Å wide anionic groove on the protein surface (indicated by *dashed arrow*). Two slices are shown that highlight the approximate dimensions of the binding groove. *D–E*, low-energy conformations of the methyl glycosides of trisaccharide **1** (*D*) and trisaccharide **2** (*E*) bound to DspB from *in silico* docking simulations.

DspB binding to methyl glycosides of trisaccharides **1** and **2** performed using Autodock Vina (46). The highest scoring docked structure for both **1** and **2** (Fig. 2, *D–E*) adopts a nearly identical conformation in which the non-reducing-end GlcNAc residue is productively positioned in the catalytic pocket in close proximity to D183 and E184. This predicted binding mode places the 2-NAc or 2-NH_3^+ group of the residue at the +2 site of **1** and **2**, respectively, within ~3.2 Å of the carboxylate oxygen of D147. Such a binding mode is consistent with the hypothesis that this amino acid facilitates recognition of cationic substrates through an electrostatic interaction.

Mutation of anionic amino acids reveals their functional role in substrate recognition

To evaluate the role of anionic amino acids on PNAG substrate recognition and turnover, we mutated residues D147, D245, and E248 to the corresponding asparagine or glutamine residue or to an alanine. We also analyzed the activity of a D183A catalytic site mutant that has been previously shown to be inactive for hydrolysis of colorimetric PNAG substrate analogs (30, 47). The effect of these mutations on DspB specificity was evaluated by analyzing reaction progress curves for the breakdown of synthetic PNAG trisaccharide analogs **1** to **4** as a function of time. As with our previous studies (33), the reactions were monitored by HPLC using the absorbance at 254 nm of the *S*-tolyl aglycone to quantify the concentration of remaining substrate and all reducing-end products. Obtaining steady-state kinetics parameters for the DspB mutants was not possible, as the K_M values for all substrates were all >5 mM and could not be directly determined due to the limited solubility of **1** to **4** (*data not shown*). Instead, we directly analyzed reaction progress curves for the enzymatic reaction measured at a single substrate concentration of 1 mM that is well below K_M for all the mutants. The observed rate k_{obs} for trisaccharide hydrolysis was determined by fitting the concentration of remaining trisaccharide substrate as a function of time to a single exponential decay using Equation 1, as summarized in Figure 3, *A–C*. Under conditions where the [S]>>K_M, the reaction velocity (v) can be accurately described by Equation 2, where the enzyme specificity constant k_{cat}/K_M is equal to the observed rate constant k_{obs}, assuming that no substrate or product inhibition is observed (48).

$$v = \left(\frac{k_{cat}}{K_M}\right)[S] \qquad (2)$$

As all of the amino acid substitutions tested in this study, with the exception of D183A, occur outside of the catalytic pocket of DspB, we can assume they will predominantly influence the substrate K_M. Thus, for the purpose of this study, it is assumed that the pseudo first-order rate constant k_{obs} is proportional to substrate binding affinity, although we cannot rule out an effect on k_{cat}. No substrate hydrolysis was observed with the D183A mutant, but with all of the other mutant enzymes tested, we observed reaction progress curves consistent with predominantly exo-glycosidic bond cleavage (Figures S2–S6). This indicates that mutations of anionic amino acids in the predicted PNAG binding surface do not appear to alter the predominant mechanism of substrate hydrolysis by DspB.

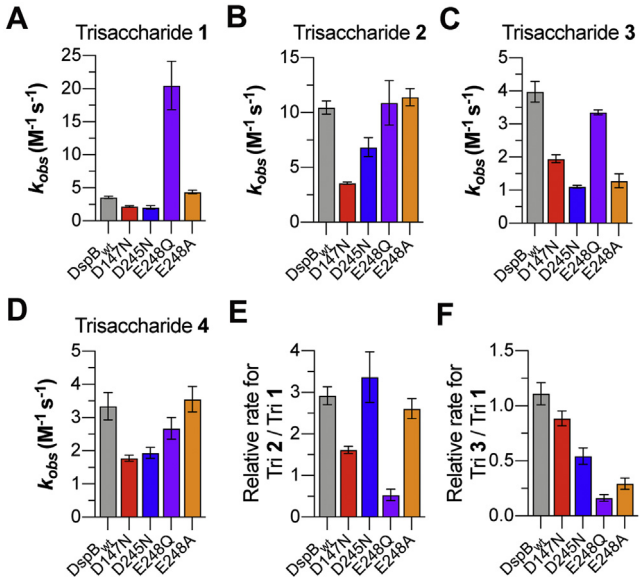

Figure 3. Observed rate of PNAG analog hydrolysis by DspB mutants. *A–D*, observed rate constants (k_{obs}) for the hydrolysis of trisaccharide **1** (*A*), **2** (*B*), **3** (*C*) and **4** (*D*) by DspB mutants determined by fitting the reaction progress curves for the disappearance of trisaccharide substrate to Equation 1. Error bars represent the 95% confidence interval from the fit of two replicate time course measurements. *E*, plot of the relative rate for each mutant with cationic trisaccharide **2** compared with fully acetylated trisaccharide **1**. *F*, plot of the relative rate for each mutant with cationic trisaccharide **3** compared with fully acetylated trisaccharide **1**.

As seen in Figure 3, *A–D*, both the D147N and D245N mutants displayed a decrease in catalytic activity with all four PNAG analogs tested; however, with the D147N mutant, the decrease in activity was greatest with cationic analog **2** as the substrate. In contrast, the D245N mutant showed only a small decrease (≤30%) relative to DspB$_{wt}$ with analogs **1**, **2**, and **4** but displayed a >threefold decrease in activity when **3** was used as the substrate. These differences can be seen most clearly when we compare the relative reaction rates for the DspB mutants with trisaccharide **2** compared with **1** (Fig. 3*E*), or with trisaccharide **3** compared with **1** (Fig. 3*F*). When we examine the relative rates, both DspB$_{wt}$ (2.9 ± 0.1) and the D245N mutant (3.2 ± 0.1) display a ~threefold increase in rate with **2** compared with **1**, whereas the D147N mutant increase is only 1.6 ± 0.1 fold. In contrast, the D245N mutant showed a nearly 50% decrease in the relative activity rate with trisaccharide **3** compared with **1**. These observations are consistent with a role of D147 in recognition of PNAG substrates containing cationic GlcN in the +2 subsite and a role for D245 in the recognition of substrates with GlcN at the +1 subsite.

Compared with the DspB D147N and D245N mutations, the activity of DspB E248Q with cationic analogs **2** and **3** or Glc containing analog **4** was statistically indistinguishable from those of DspB$_{wt}$. However, the E248Q mutant showed a >fivefold increase in catalytic activity with fully acetylated trisaccharide analog **1**. This was rather unexpected, as our hypothesis was that the mutation of anionic amino acids would predominantly affect DspB activity on cationic substrates.

Since the enhanced activity was only observed for D248Q with fully acetylated trisaccharide **1**, it may be a result of additional hydrogen bonding between the substrate *N*-acetamido group and the amide side chain of E248Q. To test this hypothesis further, we prepared an E248A mutant. The activity of DspB E248A was indistinguishable from that of $DspB_{wt}$ with trisaccharides **1**, **2**, and **4** (Fig. 3, *A*, *B* and *D*) and showed a >threefold decrease in activity with **3** (Fig. 3*C*). This data supports our hypothesis that interactions with the amide side chain of E248Q contribute to the enhanced activity observed with analog **1** and suggests that E248, like D245, predominantly interacts with cationic GlcN in the +1 subsite.

Role of anionic residues in biofilm dispersal

The substrate specificity measurements reported in Figure 3 were obtained using synthetic PNAG substrate analogs and may not accurately represent the role of these anionic amino acids in the recognition of native PNAG polysaccharides. To test this, we evaluated the D147N, D245N, D248A, and D248Q mutants for their ability to hydrolyze PNAG in an *in vitro* model of *S. epidermidis* biofilm dispersal. *S. epidermidis* RP62A is a methicillin-resistant isolate that produces robust PNAG-dependent biofilms on abiotic surfaces (16, 22, 49, 50). Here, biofilms of *S. epidermidis* RP62A that were grown in static culture for 24 h in a 96-well microtiter plate were treated with increasing concentrations of each DspB mutant and the remaining adherent biofilm biomass was quantified by crystal violet staining (Fig. 4*A*) (51, 52). After treating the biofilms for 90 min with $DspB_{wt}$, there was a quantifiable reduction in adherent biofilm biomass that was dependent on enzyme concentration. Under these conditions, a biofilm dispersal EC_{50} of 240 ± 60 pM was measured for $DspB_{wt}$ (Fig. 4*B*). Treating with the catalytically inactive D183A mutant resulted in less than 20% dispersal, even after 90 min treatment with 2.5 μM enzyme, which is consistent with this residue's role in stabilizing formation of the oxazolinium ion intermediate during PNAG hydrolysis (30). As seen in Figure 4*B*, the EC_{50} for the D147N mutant (480 ± 100 pM) was nearly twofold greater than that of $DspB_{wt}$ while those for D245N (320 ± 80 pM) and E248A (280 ± 90 pM) were the same as $DspB_{wt}$, within experimental error. This is consistent with the observed activities for these mutants with trisaccharide analogs **1** to **3**. The E248Q mutant had the lowest EC_{50} at 13 ± 4 pM, consistent with the enhanced catalytic activity observed for this mutant with fully acetylated PNAG analog **1**. The nearly 20-fold reduction of biofilm dispersal EC_{50} for the E248Q mutant is larger than the fivefold improvement of catalytic activity observed with fully acetylated PNAG analog **1**. This improved biofilm dispersal EC_{50} suggests that this mutant enzyme may partition into the biofilm to a greater extent than $DspB_{wt}$ as a result of improved substrate binding. In fact, previous studies using a green fluorescent protein–catalytically inactive DspB mutant conjugate noted that the amount of the conjugate that remained bound to cells was highly dependent

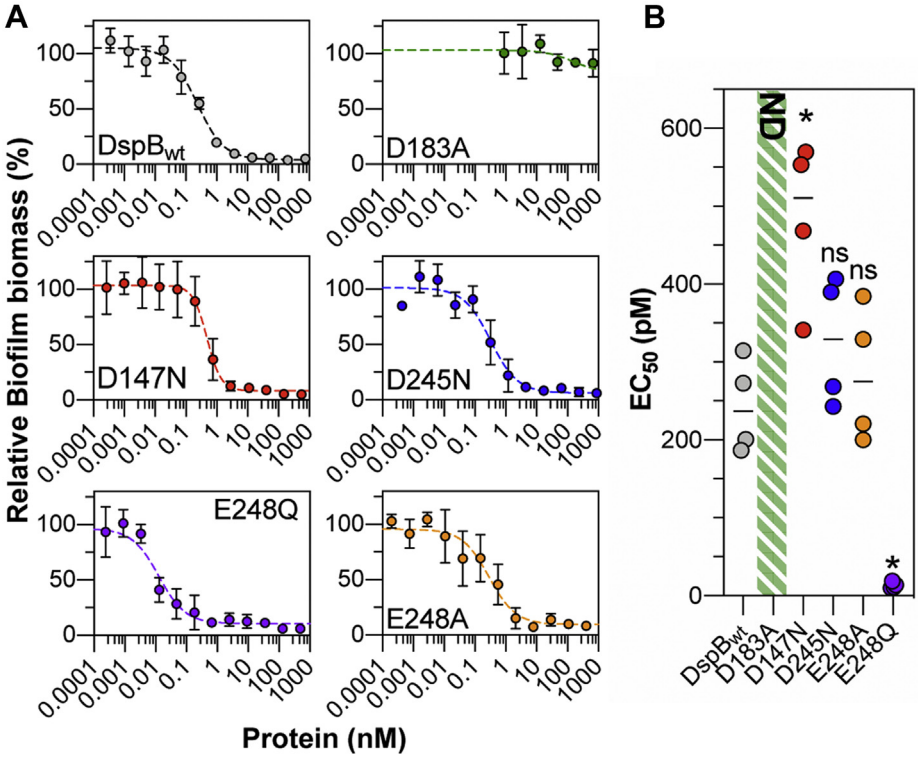

Figure 4. Dispersal of *S. epidermidis* biofilms by DspB mutants. *A*, plots of *S. epidermidis* RP62A biofilm biomass remaining after treating with varying concentrations of DspB mutants for 90 min relative to untreated biofilms. Error bars represent the standard deviation of four biological replicates. *B*, EC_{50} values from *S. epidermidis* biofilm dispersal assays from four biological replicates. Statistical significance as compared with $DspB_{wt}$ was determined using a one-way ANOVA with Dunnett's multiple comparison. *$p < 0.05$; ns, not significant. ND: the EC_{50} was not determined as >75% biofilm biomass remained even after treating with 2.5 μM enzyme for 90 min.

on the cell density (54), suggesting that PNAG binding affinity plays a critical role in the ability of DspB to partition into biofilms.

Discussion

Given the importance of PNAG for biofilm integrity and its widespread distribution among Gram-positive and Gram-negative bacteria, enzymes that catalyze the hydrolysis of PNAG are potentially useful for treating diverse biofilm infections (11, 12). Two PNAG glycosidases, DspB and the *C*-terminal domain of PgaB, have been described to date, but both suffer from relatively low catalytic activity (29, 30, 35). For example, the activity of DspB measured with a variety of substrate analogs has resulted in observed rates in the order of 2 to 60 M^{-1} s^{-1} (30, 32) nearly 4 to 6 orders of magnitude slower than comparable rates observed with other GH20 enzymes (40, 53). The poor catalytic activity of DspB likely results from the low binding affinity between DspB and its PNAG substrate. In fact, measurements of DspB binding affinity for PNAG oligosaccharides of varying lengths resulted in measured dissociation constants (K_d) of between 1 and 10 mM (54). Efforts to improve DspB catalytic efficiency would benefit from a detailed analysis of substrate binding.

Our previous studies showed that DspB has nearly threefold greater catalytic activity with substrate analog **2**, containing GlcN in the predicted +2 binding site, when compared with fully acetylated analog **1** (33). In the studies described here, we confirmed this substrate preference and demonstrated that it is the cationic charge of GlcN at the +2 site that is responsible for the increased catalytic activity. This suggests that anionic amino acid residues of DspB contribute to PNAG substrate binding. The results of *in silico* docking simulations and site-directed mutagenesis support a model of PNAG binding along a shallow anionic groove on the surface of DspB with D147 contributing to the recognition of cationic GlcN residues at the +2 site of the PNAG substrate. The modest decrease in activity observed for a D147N mutant is consistent with this role in recognition of cationic PNAG substrates, but also suggests that other residues along the substrate binding surface likely contribute to the recognition of cationic PNAG substrates at the +2 subsite as well. Moreover, the reduced activity of DspB D147N was consistent with its observed biofilm dispersal activity on PNAG-dependent *S. epidermidis* biofilms in a surface-attached biofilm model.

The activity of D245N and E248A mutants of DspB was consistent with $DspB_{wt}$ with analogs **1**, **2**, and **4**, but showed a large >threefold decrease in activity with cationic analog **3**, which contains GlcN as the central sugar. This activity is consistent with a role of D245 and E248 predominantly in the recognition of GlcN in a +1 binding site of DspB. However, the observed decrease in activity for these mutants did not result in a statistically significant decrease in their ability to disperse preformed *S. epidermidis* biofilms.

The overall results of these studies are consistent with the bound conformation of trisaccharide **1** and **2** predicted from rigid body docking simulations (Fig. 2, *D*–*E*). In these models, the nonreducing GlcNAc residue occupies the catalytic pocket in an orientation consistent with the crystal structures of related GH20 enzymes, including *Ostrinia furnacalis* Hex1 (55), *Serratia marcescens* chitobiase (39) *Bifidobacterium bifidum* lactobiase (56), *Streptococcus pneumoniae* StrH (44), and *Streptomyces plicatus* β-*N*-hexosaminidase (57). Compared with these other GH20 enzymes, the surface surrounding the catalytic pocket of DspB is shallow and lacks aromatic amino acid residues that would contribute to substrate recognition through C-H/π interactions that are present in most of the other GH20 enzymes (Fig. S1). The docked conformations of both **1** and **2** place the 2-NHAc or $-NH_3^+$ group of the +2 residue within 3.2 Å of the carboxylate oxygen of D147. Such a conformation would allow for either hydrogen bonding, in the case of **1**, or the formation of a charge–charge interaction, in the case of **2**, consistent with the reduced catalytic activity observed for the D147N mutant in this study. Moreover, this substrate binding model places the *N*-acetamido group of the central GlcNAc residue of the trisaccharide in proximity of both D245 and E248 residues of DspB.

The substrate binding model from these docking simulations appears consistent with the results of our site-directed mutagenesis studies, but it is important to note that few specific binding interactions with the PNAG substrates were observed. In fact, significant interactions were only observed between amino acids in the catalytic pocket and the −1 GlcNAc residue of the substrate and between D147 and the +2 residue, but there was a lack of other stabilizing interactions observed between DspB and the +1 and +2 residues of both docked trisaccharides **1** and **2**. The lack of specific binding interactions may explain the relatively poor binding affinity that has been observed between DspB and PNAG analogs *in vitro* (54). Interestingly, the E248Q mutant, located within the α6-helix extension that is unique to the structure of DspB, had no impact on activity with cationic substrate analogs **2** or **3**, but resulted in a fivefold increase in activity with fully acetylated analog **1**. The same activity was not observed for the neutral deacetylated analog **3**, introducing a hypothesis that the E248Q mutation introduces new substrate binding interactions unique to the fully acetylated PNAG substrates. The increased activity was not observed with an E248A mutant that lacks the side chain amide, supporting a role for hydrogen bonding between the side chain amide of E248Q and the 2-acetamido group at the +2 site of trisaccharide **1**. Such an interaction was not observed in the docked structure of **1** (Fig. 2*D*) that orients the +2 GlcNAc more than 9 Å from E248. It is important to note that these *in silico* docking simulations were performed using the DspB apo structure (PDB 1YHT) (36). It is possible that substrate binding induces a conformational change in DspB that would place E248Q in closer proximity to the bound substrate or that there is sufficient flexibility in the orientation of bound PNAG substrate that would allow it to adopt a bound conformation placing the +2 residue in closer proximity to the α6-helix extension. The first possibility, a conformational change of the α6-helix extension, is supported, at least in part, from an analysis of B-factors for the DspB apo structure (36). The α6-helix

extension and residues in the anionic binding surface have among the highest B-factors (Fig. S7) indicating these residues reside in an area of increased flexibility in the DspB apo structure. Further structural studies of DspB with PNAG substrate analogs are required to analyze any possible conformational flexibility in greater detail.

Taken together, the results of the studies presented here support a model in which PNAG binds along a shallow anionic groove on the DspB surface, and that D147 contributes to the recognition of cationic PNAG substrates containing GlcN in the +2 binding site through charge–charge interactions. Additionally, anionic amino acids D245 and E248 in the α6-helix extension interact with GlcN at the +1 binding site. However, these interactions appear to be relatively weak, having only modest effects on catalytic turnover. The poor substrate affinity of DspB for PNAG subsrates in these binding subsites might provide greater substrate flexibility in the PNAG binding site. This would allow DspB to accommodate substrates with diverse and heterogeneous PNAG modifications, such as differences in the percent de-*N*-acetylation or substrate *O*-succinylation that are known to vary depending on the bacterial species and environmental factors (16, 22). Overall, we showed that site-directed mutagenesis of residues lining this anionic binding surface can alter the catalytic turnover of PNAG substrate analogs such as **1** to **4** and that mutations that improve the catalytic efficiency of DspB with oligosaccharide substrates correlate with improved dispersal of PNAG dependent biofilms *in vitro*. Future work should focus on mutations of the residues lining the anionic binding surface to engineer DspB mutants that may function as more effective biofilm dispersal agents for treatment of diverse biofilm-dependent infections.

Experimental procedures

Protein production

Recombinant Dispersin B (residues 16–381, $DspB_{wt}$) from *A. actinomycetemcomitans* was prepared as described previously (33). Plasmids for expression of $DspB_{D183A}$ were prepared as previously described (47). Plasmids for expression of $DspB_{D147N}$, $DspB_{D245N}$, $DspB_{E248Q}$, and $DspB_{E248A}$ mutants were prepared by Quikchange site-directed mutagenesis using the primer pairs outlined in Table 1. All mutations were confirmed by single-pass Sanger sequencing and were expressed recombinantly in *E. coli* BL21(DE3) and purified as described for $DspB_{wt}$ (33). Proteins were quantified by UV absorbance at 280 nm using a calculated molar extinction coefficient of 51,340 M^{-1} cm^{-1}. All proteins were purified to >95% purity as confirmed *via* SDS-PAGE (Fig. S8), flash frozen, and stored as individual aliquots at −80 °C for later use.

Table 1
Primers for site-directed mutagenesis used in this study

DspB mutant	Primer pair
D147N	Fwd 5′- GCCGTCAAGTGGACAATGAGATCGACA TTACC
	Rev 5′- GGTAATGTCGATCTCATTGTCCACTTGACGGC
D245N	Fwd 5′- CGGTGATACCCAAAATAAAAACGAGGC GGCGG
	Rev 5′- CCGCCGCCTCGTTTTTCTGTTGGGTATCACCG
E248Q	Fwd 5′- CGAGGCGGCGCAACGTCGTGATATGCG
	Rev 5′- CGCATATCACGACGTTGCGCCGCCTCG
E248A	Fwd 5′- CGAGGCGGCGGCACGTCGTGATATGCG
	Rev 5′- CGCATATCACGACGTGCCGCCGCCTCG

Rigid body docking simulations

Trisaccharide substrate models for the methyl glycosides of **1** and **2** were prepared with the nonreducing GlcNAc residue adopting an ^4E ring conformation observed in crystal structures of related GH20 enzymes with bound substrate (39, 44, 55, 57). Models for the rest of the trisaccharide substrates were prepared using the lowest energy $^4C_1$ ring conformers and glycosidic bond conformations generated using glycan builder on the glycam.org webserver (58) and prepared using in Open Babble. Ring conformations were fixed while all other bonds were allowed to freely rotate. Rigid body docking simulations for the binding of **1** or **2** were carried out using Autodock Vina (46). The highest-scoring ligand conformers for both trisaccharides adopted the same conformation with the nonreducing terminal GlcNAc residue bound in the catalytic pocket in the same orientation as observed in other GH20 enzymes. These conformers were exported for figure preparation in Pymol (version 2.3.0).

Time course assays for hydrolysis of PNAG analogs 1 to 4

Reaction progress curves for hydrolysis of analogs **1** to **4** by DspB mutants were measured by HPLC using the previously reported approach with a few modifications (33). Briefly, hydrolysis reactions containing 1 mM of trisaccharide (**1**–**4**) in 48 mM potassium phosphate, pH 6.0 buffer containing 100 mM NaCl were initiated by the addition of an appropriate concentration of $DspB_{wt}$ or DspB mutant enzyme in a final volume of 50 μl. Individual 5 μl aliquots were removed after 0 min, 10 min, 30 min, 60 min, 90 min, 180 min, 240 min, and 360 min incubations at 22 °C and quenched through the addition of 5 μl of 100 mM trifluoroacetic acid (TFA). Quenched fractions were centrifuged at 17,000*g* for 2 min to pellet any insoluble material, diluted to 50 μl with MQ water, and analyzed by reversed-phase HPLC as described previously (33). The concentration of residual substrate and all reducing-end products were determined from their relative peak areas based on the absorbance at 254 nm resulting from the *S*-tolyl aglycone. Reaction rates for trisaccharide hydrolysis were determined by plotting the concentration of residual trisaccharide as a function of time and fitting to a single exponential using Equation 1 where [S] is the trisaccharide concentration at time *t*, $[S_o]$ is the initial trisaccharide concentration, and $[E_o]$ is the initial enzyme concentration. This gives a normalized pseudo-first-order rate constant k_{obs} in units of M^{-1} s^{-1}.

S. epidermidis *biofilm dispersal assays*

S. epidermidis RP62A was obtained from ATCC (ATCC 35984). For biofilm dispersal assays, a starter culture was grown in 25 ml of tryptic soy broth (TSB) for 24 h at 37 °C with shaking. The starter culture was then diluted to an OD_{600}

of 0.01 using sterile TSB and 200 μl of the diluted culture was added to each well of a clear, flat-bottom 96-well plate (ThermoFisher Nunc Edge). MQ water was added to the outer moat according to the manufacturer's recommendation to limit evaporation and edge effects during growth. The plates were grown in static culture for 24 h at 37 °C. After 24 h, the culture media and all nonadherent cells were removed by aspiration and 200 μl of sterile 50 mM potassium phosphate buffer, pH 6.0 was added to each well. Twenty microliter of a solution containing various dilutions of $DspB_{wt}$ or mutant enzyme in 50 mM potassium phosphate buffer, pH 6.0 was added to the wells to a final volume of 220 μl. A minimum of eight replicates on each plate were incubated with buffer alone and functioned as no dispersal controls (0% dispersal). The plates were incubated with enzyme at 25 °C for 90 min, at which time the buffer solution was removed by aspiration, and the plates were washed gently but thoroughly with DI water to remove any nonadherent biomass. Remaining adherent cells were fixed with MeOH (200 μl) for 1 h after which the wells were aspirated and allowed to fully dry. This was followed by staining with 1% crystal violet (200 μl) for 5 min. The wells were rinsed thoroughly with DI water until the water ran clear. The plates were imaged to document the stained biofilm biomass.

To quantify the adherent biomass, 200 μl of 33% acetic acid was added to each well to release the crystal violet, and 50 μl was removed and diluted with an additional 150 μl of 33% acetic acid in a separate 96 well micro-titer plate. The absorbance of crystal violet in each well was measured at 590 nm using a plate reader. The relative biofilm dispersal was calculated by dividing the absorbance at 590 nm by the average absorbance of the no dispersal control wells from each plate. The relative biofilm biomass was plotted as a function of enzyme concentration to determine EC_{50} values for biofilm dispersal. Each enzyme concentration was analyzed in quadruplicate in different positions on the 96-well plate to minimize artifacts from edge effects. Statistical significance of EC_{50} values relative to $DspB_{wt}$ were determined using a one-way ANOVA with Dunnet's multiple comparison as implemented in GraphPad Prism 8 software.

Data availability

All data supporting the findings in this study are available within the article and its supporting information.

Supporting information—This article contains supporting information (59).

Acknowledgments—We are grateful to F. Chen and Y. Li for assistant with analytical NMR and mass spectrometry services.

Author contributions—A. P. B. and C. L. produced all proteins, and A. P. B. carried out all activity and *in vitro* biofilm dispersal assays. S. W. synthesized trisaccharide substrates 1 to 3. A. P. B. and M. B. P. wrote the article. All authors analyzed data and reviewed the final version of the article.

Funding and additional information—This work was funded in part by startup funds and a Faculty Student Research Award from the Graduate School at University of Maryland College Park.

Conflict of interest—The authors declare that they have no conflicts of interest with the contents of this article. The content is solely the responsibility of the authors and does not necessarily represent the official views of the National Institutes of Health.

Abbreviations—The abbreviations used are: CAZy, Carbohydrate Active enZYmes; DspB, Dispersin B; EPS, extracellular polymeric substance; GH, glycosyl hydrolase; PNAG, poly-β-(1→6)-N-acetyl-glucosamine; TFA, trifluoroacetic acid.

References

1. Davey, M. E., and O'Toole, G. A. (2000) Microbial biofilms: from ecology to molecular genetics. *Microbiol. Mol. Biol. Rev.* **64**, 847–867
2. Flemming, H.-C., and Wingender, J. (2010) The biofilm matrix. *Nat. Rev. Microbiol.* **8**, 623–633
3. Costerton, J. W., Stewart, P. S., and Greenberg, E. P. (1999) Bacterial biofilms: a common cause of persistent infections. *Science* **284**, 1318–1322
4. Koo, H., and Yamada, K. M. (2016) Dynamic cell–matrix interactions modulate microbial biofilm and tissue 3D microenvironments. *Cur. Opin. Cell Biol.* **42**, 102–112
5. Nadell, C. D., Drescher, K., Wingreen, N. S., and Bassler, B. L. (2015) Extracellular matrix structure governs invasion resistance in bacterial biofilms. *ISME J.* **9**, 1700–1709
6. Hobley, L., Harkins, C., MacPhee, C. E., and Stanley-Wall, N. R. (2015) Giving structure to the biofilm matrix: an overview of individual strategies and emerging common themes. *FEMS Microbiol. Rev.* **39**, 649–669
7. Vuong, C., Voyich, J. M., Fischer, E. R., Braughton, K. R., Whitney, A. R., DeLeo, F. R., and Otto, M. (2004) Polysaccharide intercellular adhesin (PIA) protects *Staphylococcus epidermidis* against major components of the human innate immune system. *Cell Microbiol.* **6**, 269–275
8. Vuong, C., Kocianova, S., Voyich, J. M., Yao, Y., Fischer, E. R., DeLeo, F. R., and Otto, M. (2004) A crucial role for exopolysaccharide modification in bacterial biofilm formation, immune evasion, and virulence. *J. Biol. Chem.* **279**, 54881–54886
9. Yan, J., and Bassler, B. L. (2019) Surviving as a community: antibiotic tolerance and persistence in bacterial biofilms. *Cell Host Microbe* **26**, 15–21
10. Joo, H.-S., and Otto, M. (2012) Molecular basis of in vivo biofilm formation by bacterial pathogens. *Chem. Biol.* **19**, 1503–1513
11. Kaplan, J. B. (2014) Biofilm matrix-degrading enzymes. *Methods Mol. Biol.* **1147**, 203–213
12. Kaplan, J. B. (2010) Biofilm dispersal: mechanisms, clinical implications, and potential therapeutic uses. *J. Dent. Res.* **89**, 205–218
13. Nijland, R., Hall, M. J., and Burgess, J. G. (2010) Dispersal of biofilms by secreted, matrix degrading, bacterial DNase. *PLoS One* **5**, e15668
14. Landini, P., Antoniani, D., Burgess, J. G., and Nijland, R. (2010) Molecular mechanisms of compounds affecting bacterial biofilm formation and dispersal. *Appl. Microbiol. Biotechnol.* **86**, 813–823
15. Heilmann, C., Schweitzer, O., Gerke, C., Vanittanakom, N., Mack, D., and Götz, F. (1996) Molecular basis of intercellular adhesion in the biofilm-forming *Staphylococcus epidermidis*. *Mol. Microbiol.* **20**, 1083–1091
16. Mack, D., Fischer, W., Krokotsch, A., Leopold, K., Hartmann, R., Egge, H., and Laufs, R. (1996) The intercellular adhesin involved in biofilm accumulation of *Staphylococcus epidermidis* is a linear β-1,6-linked glucosaminoglycan: purification and structural analysis. *J. Bacteriol.* **178**, 175–183
17. Cramton, S. E., Gerke, C., Schnell, N. F., Nichols, W. W., and Götz, F. (1999) The intercellular adhesion (ica) locus is present in Staphylococcus aureus and is required for biofilm formation. *Infect. Immun.* **67**, 5427–5433

18. Wang, X., Preston, J. F., and Romeo, T. (2004) The pgaABCD locus of *Escherichia coli* promotes the synthesis of a polysaccharide adhesin required for biofilm formation. *J. Bacteriol.* **186**, 2724–2734
19. Chen, K.-M., Chiang, M.-K., Wang, M., Ho, H.-C., Lu, M.-C., and Lai, Y.-C. (2014) The role of pgaC in *Klebsiella pneumoniae* virulence and biofilm formation. *Microb. Pathog.* **77**, 89–99
20. Choi, A. H. K., Slamti, L., Avci, F. Y., Pier, G. B., and Maira-Litran, T. (2009) The pgaABCD locus of *Acinetobacter baumannii* encodes the production of poly-β-1-6-*N*-acetylglucosamine, which is critical for biofilm formation. *J. Bacteriol.* **191**, 5953–5963
21. Guo, H., and Xiang, J. (2015) Influence of poly-β-1-6-*N*-acetylglucosamine on biofilm formation and drug resistance of *Acinetobacter baumannii*. *Chin. J. Burn* **31**, 45–47
22. Sadovskaya, I., Vinogradov, E., Flahaut, S., Kogan, G., and Jabbouri, S. (2005) Extracellular carbohydrate-containing polymers of a model biofilm-producing strain, *Staphylococcus epidermidis* RP62A. *Infect. Immun.* **73**, 3007–3017
23. Itoh, Y., Wang, X., Hinnebusch, B. J., Preston, J. F., and Romeo, T. (2005) Depolymerization of β-1,6-*N*-acetyl-D-glucosamine disrupts the integrity of diverse bacterial biofilms. *J. Bacteriol.* **187**, 382–387
24. Itoh, Y., Rice, J. D., Goller, C., Pannuri, A., Taylor, J., Meisner, J., Beveridge, T. J., Preston, J. F., and Romeo, T. (2008) Roles of pgaABCD genes in synthesis, modification, and export of the *Escherichia coli* biofilm adhesin poly-β-1,6-*N*-acetyl-D-glucosamine. *J. Bacteriol.* **190**, 3670–3680
25. Kaplan, J. B., Mlynek, K. D., Hettiarachchi, H., Alamneh, Y. A., Biggemann, L., Zurawski, D. V., Black, C. C., Bane, C. E., Kim, R. K., and Granick, M. S. (2018) Extracellular polymeric substance (EPS)-degrading enzymes reduce staphylococcal surface attachment and biocide resistance on pig skin *in vivo*. *PLoS One* **13**, e0205526
26. Kaplan, J. B., Ragunath, C., Velliyagounder, K., Fine, D. H., and Ramasubbu, N. (2004) Enzymatic detachment of *Staphylococcus epidermidis* biofilms. *Antimicrob. Agents Chemother.* **48**, 2633–2636
27. Donelli, G., Francolini, I., Romoli, D., Guaglianone, E., Piozzi, A., Ragunath, C., and Kaplan, J. B. (2007) Synergistic activity of dispersin B and cefamandole nafate in inhibition of staphylococcal biofilm growth on polyurethanes. *Antimicrob. Agents Chemother.* **51**, 2733–2740
28. Kaplan, J. B., Ragunath, C., Ramasubbu, N., and Fine, D. H. (2003) Detachment of *Actinobacillus actinomycetemcomitans* biofilm cells by an endogenous β-hexosaminidase activity. *J. Bacteriol.* **185**, 4693–4698
29. Little, D. J., Pfoh, R., Mauff, F. L., Bamford, N. C., Notte, C., Baker, P., Guragain, M., Robinson, H., Pier, G. B., Nitz, M., Deora, R., Sheppard, D. C., and Howell, P. L. (2018) PgaB orthologues contain a glycoside hydrolase domain that cleaves deacetylated poly-β-(1,6)-*N*-acetylglucosamine and can disrupt bacterial biofilms. *PLoS Pathog.* **14**, e1006998
30. Manuel, S. G. A., Ragunath, C., Sait, H. B. R., Izano, E. A., Kaplan, J. B., and Ramasubbu, N. (2007) Role of active-site residues of dispersin B, a biofilm-releasing β-hexosaminidase from a periodontal pathogen, in substrate hydrolysis. *FEBS J.* **274**, 5987–5999
31. Fekete, A., Borbás, A., Gyémánt, G., Kandra, L., Fazekas, E., Ramasubbu, N., and Antus, S. (2011) Synthesis of β-(1,6)-linked *N*-acetyl-D-glucosamine oligosaccharide substrates and their hydrolysis by Dispersin B. *Carbohydr. Res.* **346**, 1445–1453
32. Fazekas, E., Kandra, L., and Gyémánt, G. (2012) Model for β-1,6-N-acetylglucosamine oligomer hydrolysis catalysed by DispersinB, a biofilm degrading enzyme. *Carbohydr. Res.* **363**, 7–13
33. Wang, S., Breslawec, A. P., Alvarez, E., Tyrlik, M., Li, C., and Poulin, M. B. (2019) Differential recognition of deacetylated PNAG oligosaccharides by a biofilm degrading glycosidase. *ACS Chem. Biol.* **9**, 1998–2005
34. Little, D. J., Poloczek, J., Whitney, J. C., Robinson, H., Nitz, M., and Howell, P. L. (2012) The structure- and metal-dependent activity of *Escherichia coli* PgaB provides insight into the partial de-N-acetylation of poly- -1,6-N-acetyl-D-glucosamine. *J. Biol. Chem.* **287**, 31126–31137
35. Forman, A., Pfoh, R., Eddenden, A., Howell, P. L., and Nitz, M. (2019) Synthesis of defined mono-de-*N*-acetylated β-(1→6)-*N*-acetyl-D-glucosamine oligosaccharides to characterize PgaB hydrolase activity. *Org. Biomol. Chem.* **17**, 9456–9466
36. Ramasubbu, N., Thomas, L. M., Ragunath, C., and Kaplan, J. B. (2005) Structural analysis of dispersin B, a biofilm-releasing glycoside hydrolase from the periodontopathogen *Actinobacillus actinomycetemcomitans*. *J. Mol. Biol.* **349**, 475–486
37. Lombard, V., Ramulu, H. G., Drula, E., Coutinho, P. M., and Henrissat, B. (2013) The carbohydrate-active enzymes database (CAZy) in 2013. *Nucleic Acids Res.* **42**, D490–D495
38. Mark, B. L., Vocadlo, D. J., Knapp, S., Triggs-Raine, B. L., Withers, S. G., and James, M. N. G. (2001) Crystallographic evidence for substrate-assisted catalysis in a bacterial β-hexosaminidase. *J. Biol. Chem.* **276**, 10330–10337
39. Tews, I., Perrakis, A., Oppenheim, A., Dauter, Z., Wilson, K. S., and Vorgias, C. E. (1996) Bacterial chitobiase structure provides insight into catalytic mechanism and the basis of Tay–Sachs disease. *Nat. Struct. Biol.* **3**, 638–648
40. Williams, S. J., Mark, B. L., Vocadlo, D. J., James, M. N. G., and Withers, S. G. (2002) Aspartate 313 in the *Streptomyces plicatus* hexosaminidase plays a critical role in substrate-assisted catalysis by orienting the 2-acetamido group and stabilizing the transition state. *J. Biol. Chem.* **277**, 40055–40065
41. Ashkenazy, H., Abadi, S., Martz, E., Chay, O., Mayrose, I., Pupko, T., and Ben-Tal, N. (2016) ConSurf 2016: an improved methodology to estimate and visualize evolutionary conservation in macromolecules. *Nucleic Acids Res.* **44**, W344–W350
42. Sumida, T., Ishii, R., Yanagisawa, T., Yokoyama, S., and Ito, M. (2009) Molecular cloning and crystal structural analysis of a novel β-*N*-acetylhexosaminidase from paenibacillus sp. TS12 capable of degrading glycosphingolipids. *J. Mol. Biol.* **392**, 87–99
43. Jiang, Y.-L., Yu, W.-L., Zhang, J.-W., Frolet, C., Guilmi, A.-M. D., Zhou, C.-Z., Vernet, T., and Chen, Y. (2011) Structural basis for the substrate specificity of a novel β-*N*-acetylhexosaminidase StrH protein from Streptococcus pneumoniae R6. *J. Biol. Chem.* **286**, 43004–43012
44. Pluvinage, B., Higgins, M. A., Abbott, D. W., Robb, C., Dalia, A. B., Deng, L., Weiser, J. N., Parsons, T. B., Fairbanks, A. J., Vocadlo, D. J., and Boraston, A. B. (2011) Inhibition of the pneumococcal virulence factor StrH and molecular insights into *N*-glycan recognition and hydrolysis. *Structure* **19**, 1603–1614
45. Kaplan, J. B., Velliyagounder, K., Ragunath, C., Rohde, H., Mack, D., Knobloch, J. K.-M., and Ramasubbu, N. (2004) Genes involved in the synthesis and degradation of matrix polysaccharide in *Actinobacillus actinomycetemcomitans* and *Actinobacillus pleuropneumoniae* biofilms. *J. Bacteriol.* **186**, 8213–8220
46. Trott, O., and Olson, A. J. (2010) AutoDock Vina: improving the speed and accuracy of docking with a new scoring function, efficient optimization, and multithreading. *J. Comput. Chem.* **31**, 455–461
47. Wang, S., Breslawec, A. P., Li, C., and Poulin, M. B. (2020) A colorimetric assay to enable high-throughput identification of biofilm exopolysaccharide-hydrolyzing enzymes. *Chem. Eur. J.* **26**, 10719–10723
48. Stroberg, W., and Schnell, S. (2016) On the estimation errors of K_M and V from time-course experiments using the Michaelis–Menten equation. *Biophys. Chem.* **219**, 17–27
49. Mack, D., Siemssen, N., and Laufs, R. (1992) Parallel induction by glucose of adherence and a polysaccharide antigen specific for plastic-adherent *Staphylococcus epidermidis*: evidence for functional relation to intercellular adhesion. *Infect. Immun.* **60**, 2048–2057
50. Christensen, G. D., Bisno, A. L., Parisi, J. T., McLaughlin, B., Hester, M. G., and Luther, R. W. (1982) Nosocomial septicemia due to multiply antibiotic-resistant *Staphylococcus epidermidis*. *Ann. Intern. Med.* **96**, 1
51. O'Toole, G. A., and Kolter, R. (1998) Initiation of biofilm formation in *Pseudomonas fluorescens* WCS365 proceeds via multiple, convergent signalling pathways: a genetic analysis. *Mol. Microbiol.* **28**, 449–461
52. Stepanović, S., Vuković, D., Dakić, I., Savić, B., and Švabić-Vlahović, M. (2000) A modified microtiter-plate test for quantification of staphylococcal biofilm formation. *J. Microbiol. Methods* **40**, 175–179
53. Vocadlo, D. J., and Withers, S. G. (2005) Detailed comparative analysis of the catalytic mechanisms of β-*N*-acetylglucosaminidases from families 3 and 20 of glycoside hydrolases. *Biochemistry* **44**, 12809–12818
54. Eddenden, A., Kitova, E. N., Klassen, J. S., and Nitz, M. (2020) An inactive dispersin B probe for monitoring PNAG production in biofilm formation. *ACS Chem. Biol.* **15**, 1204–1211

55. Liu, T., Zhang, H., Liu, F., Wu, Q., Shen, X., and Yang, Q. (2010) Structural determinants of an insect β-*N*-acetyl-D-hexosaminidase specialized as a chitinolytic enzyme. *J. Biol. Chem.* **286**, 4049–4058
56. Ito, T., Katayama, T., Hattie, M., Sakurama, H., Wada, J., Suzuki, R., Ashida, H., Wakagi, T., Yamamoto, K., Stubbs, K. A., and Fushinobu, S. (2013) Crystal structures of a glycoside hydrolase family 20 lacto-*N*-biosidase from *Bifidobacterium bifidum*. *J. Biol. Chem.* **288**, 11795–11806
57. Mark, B. L., Wasney, G. A., Salo, T. J. S., Khan, A. R., Cao, Z., Robbins, P. W., James, M. N. G., and Triggs-Raine, B. L. (1998) Structural and functional characterization of Streptomyces plicatus β-N-acetylhexosaminidase by comparative molecular modeling and site-directed mutagenesis. *J. Biol. Chem.* **273**, 19618–19624
58. Woods Group (2005-2020) *GLYCAM Web*, Complex Carbohydrate Research Center, University of Georgia, Athens, GA
59. Ren, B., Cai, L., Zhang, L.-R., Yang, Z.-J., and Zhang, L.-H. (2005) Selective deacetylation using iodine–methanol reagent in fully acetylated nucleosides. *Tetrahedron Lett.* **46**, 8083–8086